Modeling and Control of a Three Level DCI in a Grid Connection Photovoltaic/Battery Storage System

K. Himour*‡, K. Ghedamsi*, E.M. Berkouk**

*Laboratory of Renewable Energy Mastery, University of Bejaia. Algeria

**Control Process Laboratory, ENP of Algiers, Algeria

(Himour.kamal@hotmail.fr, kghedamsi@yahoo.fr, emberkouk@yahoo.fr)

‡Corresponding Author; Kamal Himour, Laboratory of Renewable Energy Mastery, University of Bejaia. Algeria, Himour.kamal@hotmail.fr

Received: 17.04.2013 Accepted: 03.06.2013

Abstract- This paper aimed to evaluate the use of a photovoltaic-battery storage system to supply electric power in the distribution grid through a multilevel inverter. A DC-DC converter is used to interface a photovoltaic (PV) generator and a lead-acid battery bank to a common DC-link. Maximum Power Point Tracker (MPPT) that allows extraction of maximum available power from the photovoltaic (PV) panels has been included. This MPPT is based on Perturb and observe method. A three level diode clamped inverter is connected to the grid by a traditional three phase transformer. To generate proper multilevel voltage waveforms, a fast and simplified space vector modulation is adopted. The proposed control scheme ensures the injection of a reference power in the distribution grid and controls the reactive power with fast dynamic response. The validation of the proposed system is proved by simulation of the whole system using MATLAB-Simulink software.

Keywords- Photovoltaic generator, MPPT, Battery bank, three level diode clamped inverter, space vector modulation, and grid utility

1. Introduction

With the increasing concern about global environmental protection, the need to produce pollution-free natural energy such as solar energy has received great interest as an alternative source of energy for the future since solar energy is clean, pollution-free and inexhaustible. In an effort to use the solar energy effectively, a great deal of research has been done on the grid-connected photovoltaic generation systems. In PV systems connected to the grid, the inverter that converts the output direct current (DC) of the solar modules to the alternate current (AC) is receiving increased interest in order to generate power to utility. Generally, the grid connected PV systems extract maximum power from the PV arrays. The maximum power point tracking (MPPT) technique is usually associated with a DC–DC converter. The DC–AC converter injects sinusoidal current into the grid, controlling the power factor [1–4].In order to inject power on demand, certain energy storage devices must be added into the system. These devices must store PV energy in excess of electricity demand and subsequently meet electricity demand in excess of PV energy. The conventional lead–acid battery is the most common energy storage device at the present time [5].Another very important aspect of the systems connected to the grid is to select a proper power factor according to the grid demands: active or reactive power. The most efficient systems are those, which allow variation in the active and reactive power injected into the grid, depending on the power grid requirements [6]. In this scenario, we propose a control strategy for a photovoltaic- battery storage system connected to the grid with a three level diode clamped inverter.

The proposed control strategy is capable of controlling, not only the current injected into the grid, but also the power factor (PF). Varying the PF, within a certain range, the injected reactive power can be dynamically changed and controlled.The paper is organized as follow: in section 2 we

presented the the system model and control: mathematical model of the photovoltaic generator, Maximum Power Point Tracker, model of battery bank, model and control of the three level diode clamped inverter, control of the global system. Then, in section 3 we presented the simulation results and we terminated by a conclusion of this study in section 4.

2. System Model and Control

Fig. 1 shows the configuration of the grid-connected PV battery storage system, which consists of PV panels, DC/DC converters for MPPT, a battery bank connected to the DC bus by a bidirectional DC-DC converter and the three level diode clamped inverter connected to the grid through a traditional three phase transformer.

The control structure of the grid-connected PV – battery storage system is composed of three structure control:

1. The MPPT Control, which the main property is to extract the Maximum power from the PV generator.
2. The inverter control, which have the main goal:

   -control the active injected into the grid;

   -control and regulate the reactive power;

   -ensure high quality of the injected power;

   -grid synchronization.

3. The DC bus control witch has the goal to regulate the DC bus and to control the charge and discharge of battery storage.

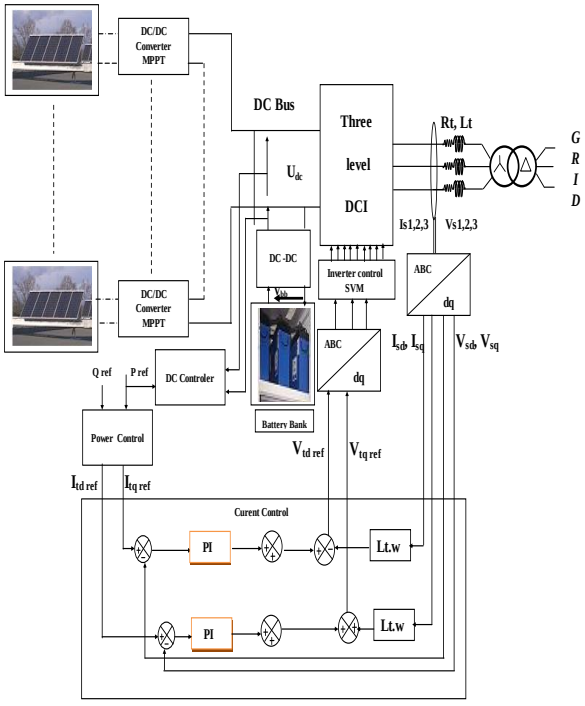

Fig. 1. Bloc diagram of the current control.

2.1. Model of PV Generator

The PV generator consists of electrically connected PV modules and it is modeled by physical oriented equivalent circuits, including one or more diode. The single diode equivalent circuit as shown in Fig. 2 is the most commonly used model for large PV generators [7].

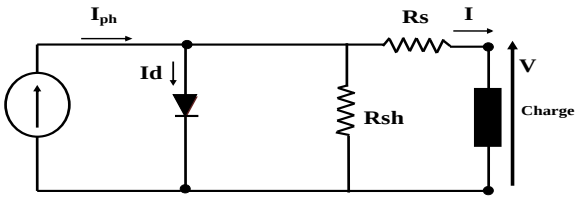

Fig. 2. Photovoltaic cell equivalent circuit.

Starting from the widely known photovoltaic cell electrical equivalent circuit, an equivalent model for a more powerful PVG made of an (Ns x Np) array of PV cells, is established [4]:

The mathematical model witch relates the output current to the output voltage is given by the following expression:

$$I = I_{ph} - I_s\left[\left(exp\frac{V+I.R_s}{m.\frac{K.T}{q}}\right) - 1\right] - \frac{V+I.R_s}{R_{sh}} \quad (1)$$

Where:

$\mathbf{I_{ph}}$: The photo-current, $\mathbf{I_s}$: the saturation current of diode, m: ideality factor, $\mathbf{R_s}$ and $\mathbf{R_{sh}}$: series and parallel resistance, T: junction temperature, K: Boltzmann constant, q : electron charge.

For a PV module with Ns series connected cells and Np parallel connected cells, the current-voltage characteristic is given by:

$$I = N_p.I_{ph} - N_p.I_s\left[exp\left\langle\left(\frac{1}{m.K.\frac{T}{q}}\right).\left(\frac{V}{N_s} + \frac{R_s.I}{N_p}\right)\right\rangle - 1\right] - \frac{N_p}{R_{sh}}.\left(\frac{V}{N_s} + \frac{R_s.I}{N_p}\right) \quad (2)$$

2.2. Maximum Power Point Tracking

The PV array must operate electrically at a certain voltage which corresponds to the maximum power point under the given operating conditions. To do this, a maximum power point tracking (MPPT) technique should be applied. Various MPPT techniques like look-up table methods, perturbation and observation (P & O) methods and computational methods have been proposed in the literature. The perturb and observe(P&O), as the name itself states that the algorithm is based on the observation of the array output power and on the perturbation (increment or decrement) of the power based on increments of the array voltage or current. The algorithm continuously increments or decrements the reference current or voltage based on the value of the previous power sample. The P&O is the simplest method which senses the PV array voltage and the cost of implementation is less and hence easy to implement [8].

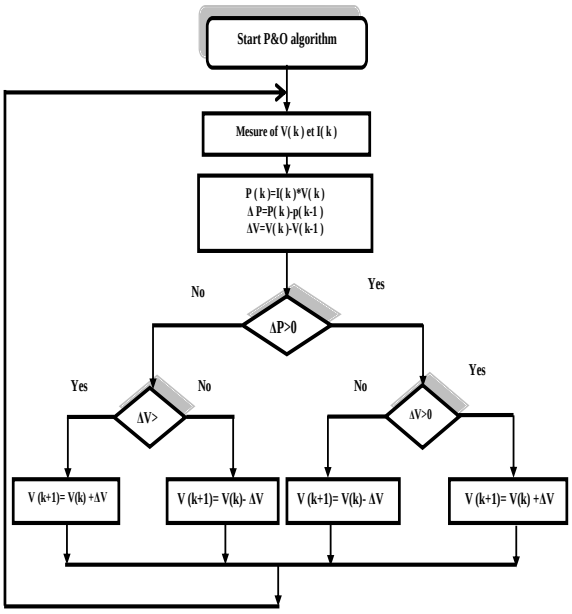

Fig. 3. Flowchart of P&O algorithm.

2.3. Battery Bank Model

Lead acid batteries are used to guarantee several hours to a few days of energy storage. The model representation of the lead-acid battery is shown in Fig. 4. The capacity of the battery is determined by integrating the main reaction current I_{MR} . To consider the increased gassing losses when charging the battery at high voltage and temperature, here represented by the loss-currentI_{gas}, constitutes a significant improvement over alternative battery models for the simulation of hybrid energy systems. The state-of-charge can be calculated by referring the actual capacity to the rated capacity of the battery, as expressed by equation 2 [9-10].

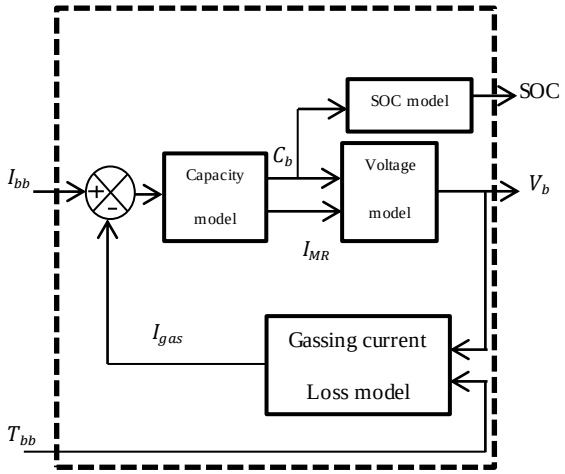

Fig. 4. General structure of battery model.

The main reaction current of the battery bank can be expressed as:

$$I_{MR}(t) = I_{bb}(t) - I_{gas}(t) \quad (3)$$

Where:

I_{MR} : Main battery reaction current (A)

I_{bb}: External battery current (A)

I_{gas}: Battery gassing current (A)

The capacity model of the battery does not limit the charge or discharge current. Operation of the system with excessive charge or discharge currents has to be prevented by the selection of appropriately sized components and the implementation of a suitable control strategy. The actual battery capacity can be determined as:

$$C_b(t) = \int_{t=0}^{t} I_{MR}(t)dt + C_{b,i} \quad (4)$$

Where:

C_b: Actual battery capacity (Ah)

$C_{b,i}$: Initial battery capacity (Ah)

The state-of-charge can be calculated by referring the actual capacity to the rated capacity of the battery:

$$SOC(t) = \frac{C_b(t)}{C_{10}} \times 100\% \quad (5)$$

The presented voltage model of the battery is based on the 'Expanded Kinetic Battery Model', which has been presented in [9].

The voltage model considers that the battery terminal voltage depends on the following factors:

- Battery state-of-charge;

- Internal battery resistance;

- Magnitude and direction of battery current

For all calculations shown, different model parameters represent the characteristic voltage behavior of lead-acid batteries when charging or discharging. The internal battery voltage is calculated as:

a) Charging ($I_{bb} < 0$)

$$E_b(t) = E_{0,c} + A_c.X(t) + \frac{C_c.X(t)}{(D_c - X(t))^{EFC}} \quad (6)$$

b) Discharging ($I_{bb} > 0$)

$$E_b(t) = E_{0,d} + A_D.X(t) + \frac{C_d.X(t)}{(D_d - X(t))^{EFd}} \quad (7)$$

Where:

E_b: Internal battery voltage (V),

X: Normalized maximum charge/discharge capacity (Ah),

The normalized maximum charge/discharge capacity X is given as:

a) Charging ($I_{bb} < 0$)

$$X(t) = \frac{Q_{max,c}}{Q_{max}.(I_{MR}(t))} C_b(t) \quad (8)$$

b) Discharging ($I_{bb} > 0$)

$$X(t) = \frac{Q_{max,d}\cdot\left(Q_{max,d} - C_b(t)\right)}{Q_{max}\cdot(I_{MR}(t))} \quad (9)$$

The maximum capacity Q_{max}in dependence of the main reaction current of the battery is expressed by a third order polynomial equation, where the parameters have to be determined by empirical curve fitting from measured data :

a) Charging ($I_{bb} < 0$)

$$Q_{max}\left(I_{MR}(t)\right) = C_1.I_{MR}(t)^3 + C_2 I_{MR}(t)^2 + C_3 I_{MR}(t) + C_4 \quad (10)$$

b) Discharging ($I_{bb} > 0$)

$$Q_{max}\left(I_{MR}(t)\right) = D_1.I_{MR}(t)^3 + D_2 I_{MR}(t)^2 + D_3 I_{MR}(t) + D_4 \quad (11)$$

Therefore, the battery terminal voltage V_b can be calculated as:

a) Charging ($I_{bb} < 0$)

$$V_b(t) = E_b(t) - R_{0,c} I_{MR}(t) \quad (12)$$

b) Discharging ($I_{bb} > 0$)

$$V_b(t) = E_b(t) - R_{0,d} I_{MR}(t) \quad (13)$$

The voltage of a string of batteries is given by multiplying the battery voltage with the number of 12 Volt batteries in series:

$$V_{bb}(t) = B_s.V_b(t) \quad (14)$$

Where:

V_{bb}: Voltage of battery bank (V),

B_s: Number of 12 V batteries in series,

2.4. Model and Control of the Three Level DCI

Multilevel converter gives massive advantages compared with conventional and very well-known two level converters like; high power quality waveforms, low switching losses, high voltage capability, low electromagnetic compatibility (EMC) etc. At the present time, the majority of research and development effort seems to concentrate on the development of three classes of inverters: the diode-clamped multilevel inverter, the multilevel inverter with cascaded single-phase H-bridge inverters and the multilevel inverter known as the flying capacitor inverter or some-times as the imbricate cells multilevel inverter [11-13].

2.4.1. Model of the three level DCI

A three-phase three-level diode-clamped inverter is shown in Fig. 5 [14].Each leg is composed of two upper and lower switches with anti-parallel diodes. Two series dc link capacitors split the dc bus voltage in half and six clamping diodes confine the voltages across the switch within the voltages of the capacitors. The necessary conditions for the switching states are that the dc link capacitors should not be shorted and the output current should be continuous.

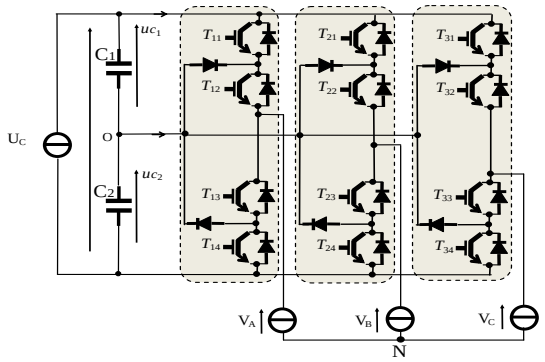

Fig. 5. Three level diode clamped inverter (DCI).

2.4.1.1. Connection functions

For each leg of the inverter, we define three connection functions, each one is associated to one of the three states of the leg:

$$\begin{cases} F_{c1j} = F_{1j}.F_{2j} \\ F_{c2j} = F_{2j}.F_{3j} \\ F_{c3j} = F_{3j}.F_{4j} \end{cases} \quad (15)$$

Table 1. The states of one leg of the 3 level DCI.

F_{k1}	F_{k2}	F_{k3}	F_{k4}	V_k	Etat
0	0	1	1	-Uc/2	N
0	1	1	0	0	O
1	1	0	0	Uc/2	P
1	0	0	1	unknown	-

As indicated in table 1, each leg of the inverter can have three possible switching states P,O N.

2.4.1.2. Output voltages

The output voltages of a three level diode clamped inverter are expressed as follows:

$$\begin{bmatrix} V_{10} \\ V_{20} \\ V_{30} \end{bmatrix} = \begin{bmatrix} F_{c11} & F_{c21} & F_{c31} \\ F_{c12} & F_{c22} & F_{c32} \\ F_{c13} & F_{c23} & F_{c33} \end{bmatrix} . \begin{bmatrix} \frac{Uc}{2} \\ 0 \\ \frac{-Uc}{2} \end{bmatrix} \quad (16)$$

From the output voltages V_{10}, V_{20} et V_{30} , we define the output voltage vector given by :

$$V_s = V_{10}e^{j0} + V_{20}e^{-j2\pi/3} + V_{30}e^{j2\pi/3} \quad (17)$$

$$\mathrm{V_s} = \mathrm{V_d} + \mathrm{j}\,\mathrm{V_q} \quad (18)$$

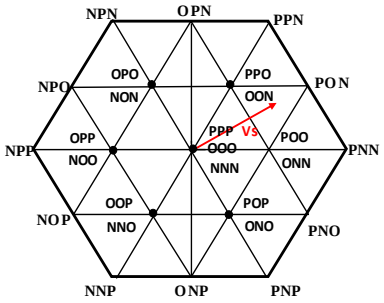

Fig. 6. Three level diode clamped inverter space vector diagram.

Fig. 6 shows the space vector diagram of the three level inverter. The output voltage space vector is identified by combination of switching states P, O, N of the three legs. Since three kinds of switching states exist in each leg, three level inverter has $3^3 = 27$ switching states.

2.4.2. Simplified spave vector pulse with modulation

In SVPWM method the output voltage is approximated by using the nearest three output vectors that the nodes of the triangle containing the reference vector changes from one region to another, it may induce an output vector abrupt change. In addition we need to calculate the switching sequences and switching time of the states at every change of the reference voltage location. In this paper, a new method is proposed in which the three level inverter is decomposed into six space vector diagrams of two level inverters (Fig. 7). This modification can reduce considerably the computational time and reduce the algorithm complexity [14].

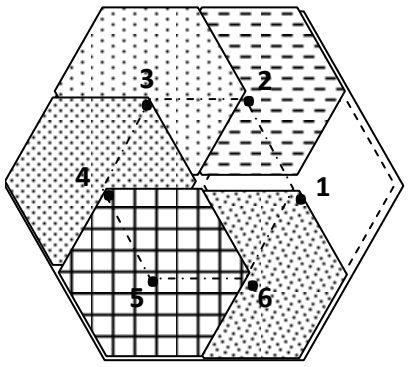

Fig. 7. Decomposition of the three level diode clamped inverter space vector diagram into six space vector diagrams of two level inverters.

2.4.2.1. Correction of reference voltage vector

Having the location of a given reference voltage vector, one hexagon is selected among the six small hexagons that contain the three level space vector diagram. Each hexagon is identified by a number s defined as given by:

$$s = \begin{cases} 1 \text{ si } \frac{-\pi}{3} \le \theta \le \frac{\pi}{3} \\ 2 \text{ si } \frac{\pi}{3} \le \theta \le \frac{\pi}{2} \\ 3 \text{ si } \frac{\pi}{2} \le \theta \le \frac{5.\pi}{6} \\ 4 \text{ si } \frac{5.\pi}{6} \le \theta \le \frac{7.\pi}{6} \\ 5 \text{ si } \frac{7.\pi}{6} \le \theta \le \frac{3.\pi}{2} \\ 6 \text{ si } \frac{3.\pi}{2} \le \theta \le \frac{11.\pi}{6} \end{cases} \quad (19)$$

After selection of one hexagon, we make a translation of the reference vector V_s^* towards the center of this hexagon

Table 2. Correction of reference voltage vector.

Hexagon	$V_d^{*\prime}$	$V_q^{*\prime}$
1	$V_d^* - 1/2$	V_q^*
2	$V_d^* - 1/4$	$V_q^* - \sqrt{3}/4$
3	$V_d^* + 1/4$	$V_q^* - \sqrt{3}/4$
4	$V_d^* + 1/2$	V_q^*
5	$V_d^* + 1/4$	$V_q^* + \sqrt{3}/4$
6	$V_d^* - 1/4$	$V_q^* + \sqrt{3}/4$

2.4.2.2. Determination of dwelling times

Ones the corrected reference voltage$\grave{V}_s^{*\prime}$ and the corresponding hexagon are determined, we can apply the conventional two level space vector PWM method to calculate the dwelling times, the only difference between the two level SVPWM and the three level SVPWM is the factor 2 appearing at the first two equations as shown in this equation:

$$\begin{cases} T_1 = 2 * \left[\frac{\left|\overrightarrow{V_s^{*\prime}}\right| . T_s . \sin(\frac{\pi}{3} - \alpha)}{\sin(\frac{\pi}{3})} \right] \\ T_2 = 2 * \left[\frac{\left|\overrightarrow{V_s^{*\prime}}\right| . T_s . \sin(\alpha)}{\sin(\frac{\pi}{3})} \right] \\ T_3 = T_s - T_1 - T_2 \end{cases} \quad (20)$$

2.4.2.3. Conversion and sequence of the switching states

The reference voltage vector $\grave{V}_s^{*\prime}$ is approximated using the nearest three states which are nodes of the triangle containing the vector identified as X, Y and Z. the optimum sequence of these states is selected so as to minimize the total number of switching transitions. It's well known that these sequences should be reversed in the next switching interval for minimum harmonic impact as given in [14].

2.5. Control System Structure

The control structure is composed of three main blocs: the DC link regulation bloc, the power control bloc and the current control bloc as shown in Fig. 8 [15, 16].

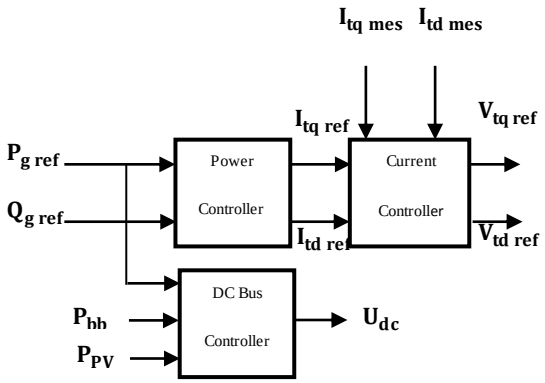

Fig. 8. Bloc diagram of the control structure.

2.5.1. *DC bus control*

The DC voltage control regulates the DC bus. Fig. 9 shows the bloc diagram of DC voltage control.

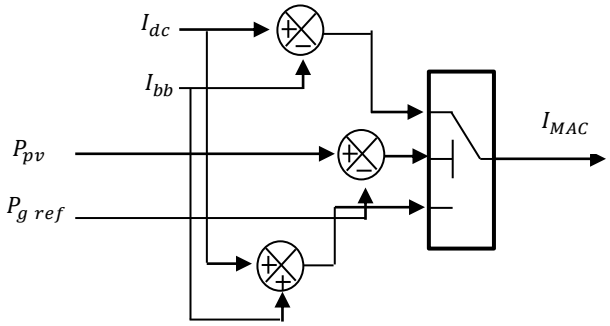

Fig. 9. Bloc diagram of the DC bus control.

Where I_{MAC} is the current in DC bus capacitor and I_{bb} is the battery bank current.

2.5.2. *Power control*

The active and reactive power (P_g, Q_g) can be both expressed by using Park components of supply voltage (V_{td}, V_{tq}) and line current (I_{td}, I_{tq}) as follows :

$$\begin{cases} P_g = V_{td}.I_{td} + V_{tq}.I_{tq} \\ Q_g = V_{td}.I_{tq} - V_{tq}.I_{td} \end{cases} \quad (21)$$

Reference currents ($I_{td\ ref}, I_{tq\ ref}$) which allows setting the desired reference active and reactive powers ($P_{g\ ref}, Q_{g\ ref}$), as follows:

$$\begin{cases} I_{td\ ref} = \frac{P_{g\ ref}.\hat{V}_{td} - Q_{g\ ref}.\hat{V}_{tq}}{\hat{V}_{td}^{\ 2} + \hat{V}_{tq}^{\ 2}} \\ I_{tq\ ref} = \frac{P_{g\ ref}.\hat{V}_{tq} + Q_{g\ ref}.\hat{V}_{td}}{\hat{V}_{td}^{\ 2} + \hat{V}_{tq}^{\ 2}} \end{cases} \quad (22)$$

The unity power factor is obtained simply by setting the reactive power reference null. We can also generate or absorb ($Q_{g\ ref} < 0\ or\ Q_{g\ ref} > 0$).

2.5.3. *Current control*

The vector current control in Park reference frame is carried out by using the synchronized reference with the grid voltage. The electric equations of the filter (R_t, L_t) connected to the grid are given bellow:

$$\begin{cases} V_{td} = R_t I_{td} + L_t \frac{dI_{td}}{dt} - \omega_s L_t I_{td} + V_{gd} \\ V_{tq} = R_t I_{tq} + L_t \frac{dI_{tq}}{dt} + \omega_s L_t I_{tq} + V_{gq} \end{cases} \quad (23)$$

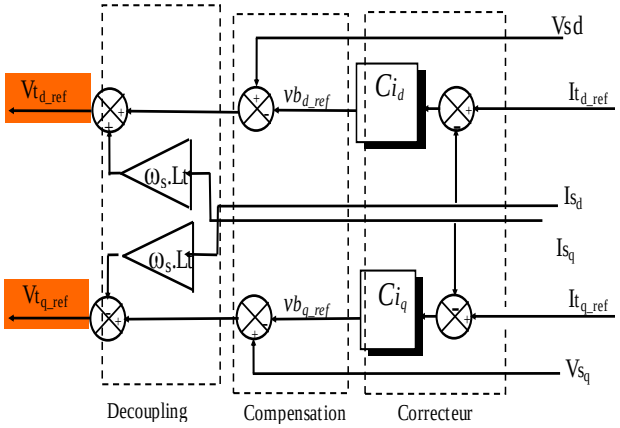

Fig. 10. Bloc diagram of the current control.

3. Result Simulation

In this section, the photovoltaic grid connexion system is simulated using SIMULINK-MATLAB. We simulate the system for two cases:

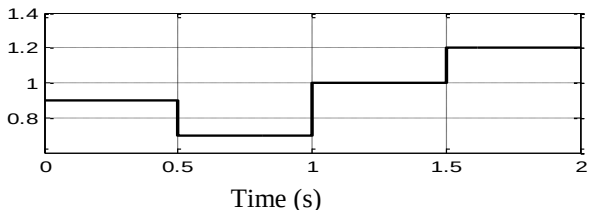

Fig. 11. Irradiance profile (sun).

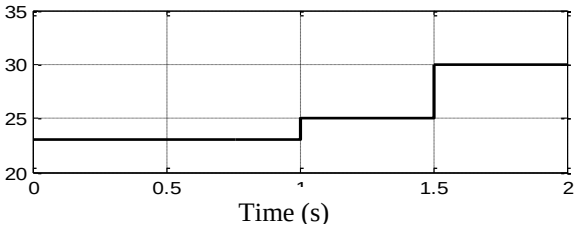

Fig. 12. Temperature (^{0}C).

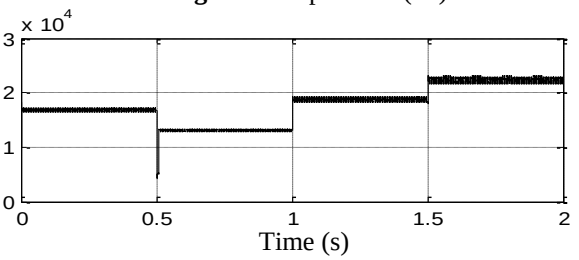

Fig. 13. Temperature (^{0}C).

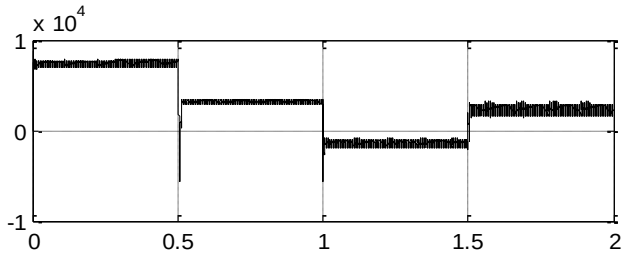

Fig. 14. Battery bank power (W).

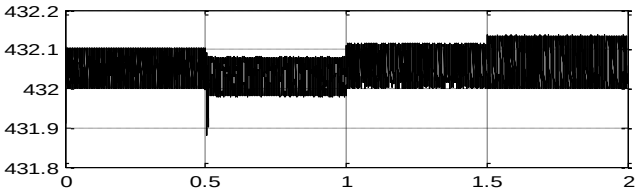

Fig. 15. DC bus voltage (V).

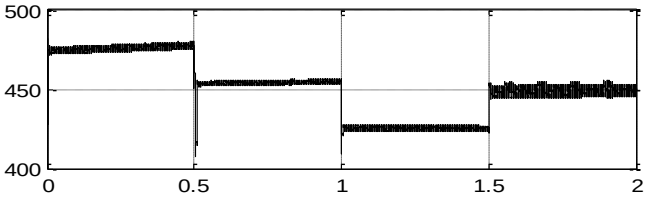

Fig. 16. DC bus voltage (V).

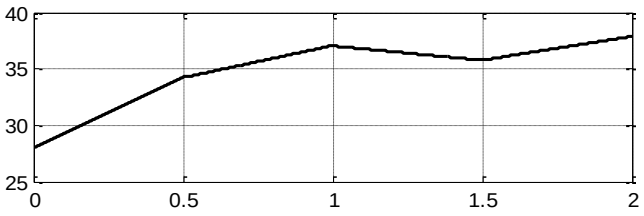

Fig. 17. State of Charge.

- **case 1 : step change of Pg ref from 10 kw to 20 kw at 1s and Qg ref = 0**

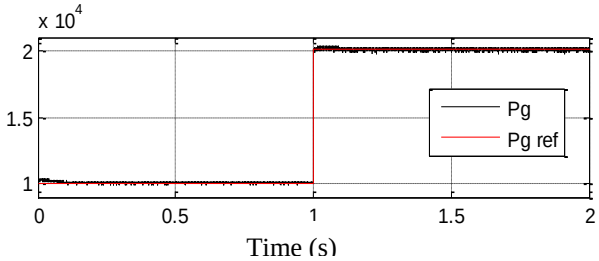

Fig. 18. Grid active power (W).

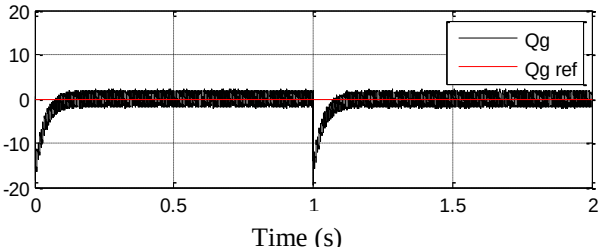

Fig. 19. Grid reactive power (var).

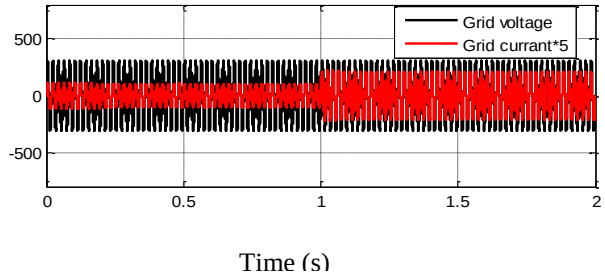

Fig. 20. Grid voltage (V) and current (A) of phase 1.

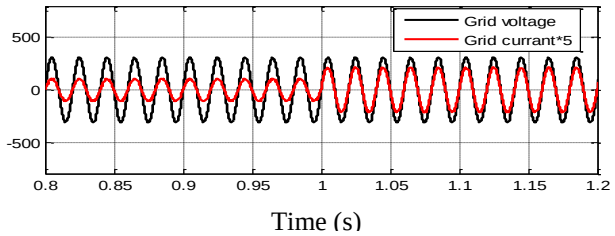

Fig. 21. Zoom of grid voltage (V) and current (A) of phase 1.

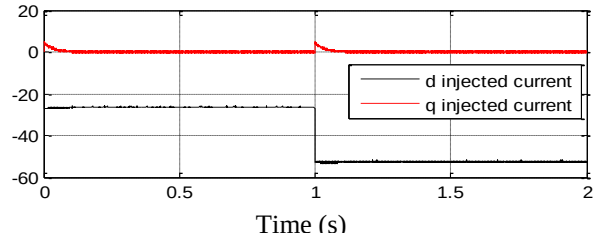

Fig. 22. d,q components of injected currant (A).

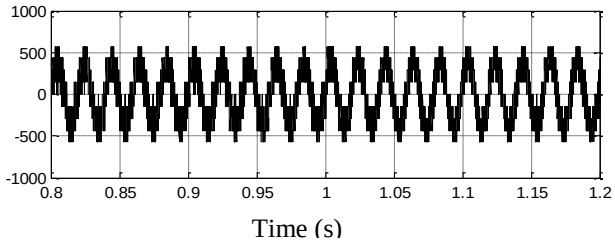

Fig. 23. Output 3 level DCI voltage phase 1 (V).

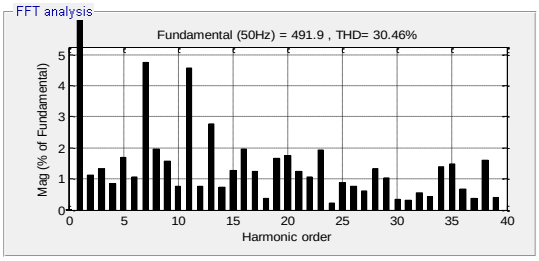

Fig. 24. THD of Output 3 level DCI voltage phase 1 (V).

- **case 2 : step change of Pg ref from 10 kw to 20 kw at 1s step change of Qg ref from -5 kw to 5 kw at 1s**

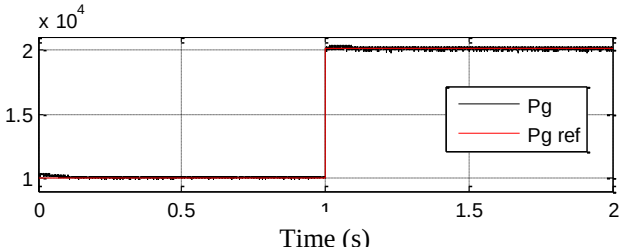

Fig. 25. Grid active power (W).

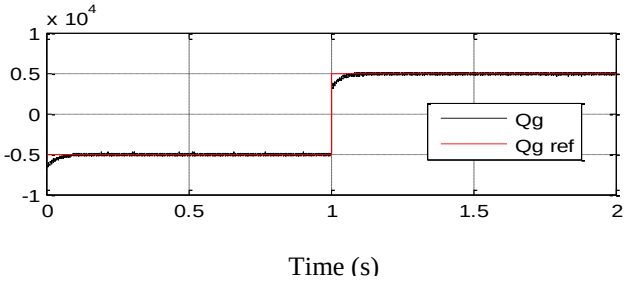

Fig. 26. Grid reactive power (var).

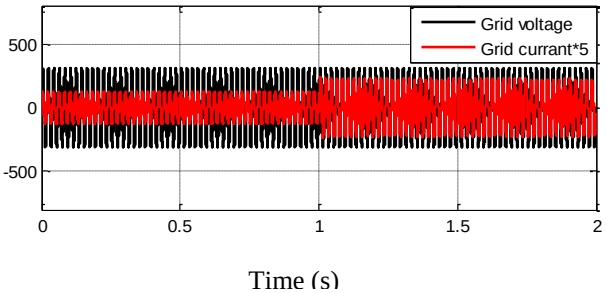

Fig. 27. Grid voltage (V) and current (A) of phase 1.

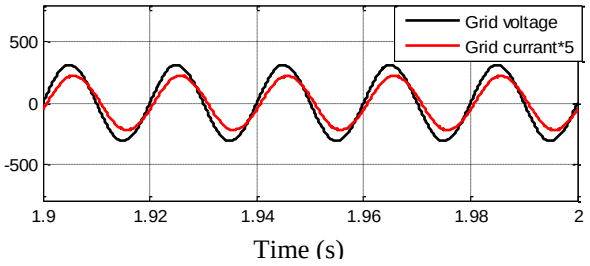

Fig. 28. Zoom of grid voltage (V) and current (A) of phase 1.

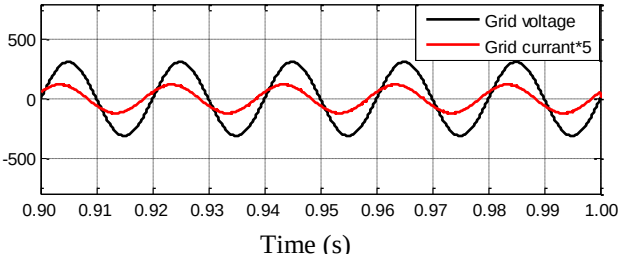

Fig. 29. Zoom of grid voltage (V) and current (A) of phase 1.

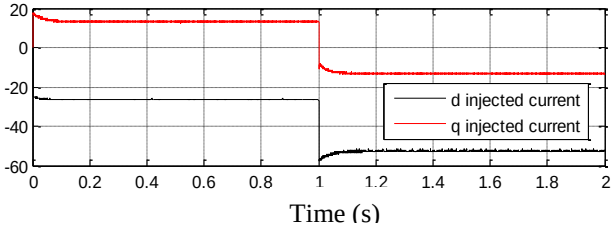

Fig. 30. d,q components of injected currant (A).

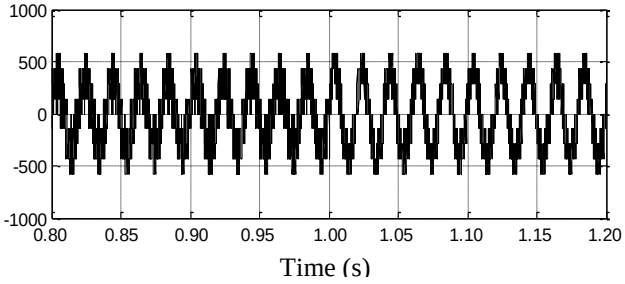

Fig. 31. Output 3 level DCI voltage phase 1 (V).

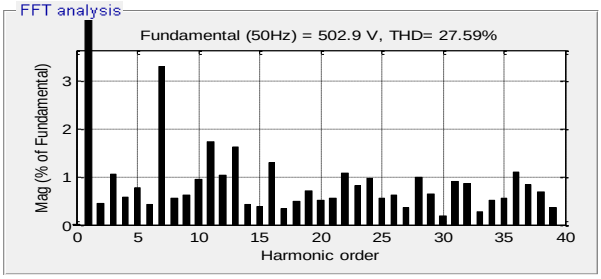

Fig. 32. THD of Output 3 level DCI voltage phase 1 (V).

These simulations improve the validity of the proposed control strategy for the grid PV/battery storage system. The results show that it is possible to inject to the grid a fixed power whatever solar irradiance and temperature condition. When the photovoltaic generator power is more than the reference power to inject into the grid, the control system ensures the multilevel inverter to inject to the grid the reference active power, the surplus energy is stocked in the battery bank and when it is less than the reference power, the battery bank compensates the difference power.

In the first case Fig. 20 and Fig. 21 show that the grid current and the grid voltage are in phase. Also, Fig. 18 and Fig. 19 show that we have injected into the grid the reference power with a unit power factor , in Fig. 23 the output voltage of the three level inverter changes when the reference power changes because the reference voltage given by the control system are changed . In the second case, the grid and current voltage are not in phase (Fig. 28, Fig. 29) because we have changed in reference reactive power (Fig. 26) .We note also that the DC bus voltage remains fixed in the two cases by the control system (Fig. 15) .The three level DCI generate output voltages in three levels and gives a good power quality into the grid.

4. Conclusion

This paper proposed the study and the control of photovoltaic-Battery storage grid connected system, the use of a three level DCI with his simplified space vector modulation as a grid interface gives a good results in term of THD and power quality, also, the aim was in this work to inject to the grid a fixed power whatever solar irradiance and temperature condition. The results obtained from this performance analysis confirm that the control strategy adopted achieves the specified performance objectives.

Appendix

Photovoltaic array			
Pmax	150	W	Maximal power
Vop	34.5	V	Optimal voltage
Iop	4.35	A	Optimal current
Voc	43.5	V	open circuit voltage
Icc	4.75	A	Short circuit current
Ns	18	1	Number of series arrays
Np	10	10	Number of parallel arrays
DC Bus			
Udc	432	V	DC bus voltage
Filter			
Rt	3	Ω	Filter resistance
Lt	0,01	H	Filter inductance
Grid			
Vs	380	V	voltage
f	50	Hz	frequency
Battery bank			
C_{10}	118	Ah	Battery capacity at 10-hour discharge rate
C_V	8	V^{-1}	Voltage coefficient
C_T	0.05	K^{-1}	Temperature coefficient
I_{G0}	0.035	A	Normalised gassing current
$Q_{max,C}$	120	Ah	Maximum charge capacity
$Q_{max,D}$	130	Ah	Maximum discharge capacity
$R_{I,C}$	75	mΩ	Internal resistance when charging the battery
$R_{I,D}$	38	mΩ	Internal resistance when discharging the battery
$E_{0,C}$	11.6	V	Limiting internal battery voltage for zero current and fully dischargedbattery after the initial transient
A_C	0.01	-	Parameter reflecting the initial linear variation of the internal battery voltage with increasing state-of-charge
C_C	0.012	-	Parameter reflecting increasing voltage when battery is progressively charged
D_C	130	-	Parameter reflecting sharp increase of voltage when battery is charged to a high SOC
EF_C	0.45	-	Exponential factor introduced to achieve a closer curve fit for voltage behaviour when progressively charged
$E_{0,d}$	12.6	V	Fully charged internal battery voltage when discharging after the initial transient
A_D	-0.007	-	Parameter reflecting the initial linear variation of the internal battery voltage with decreasing state-of-charge
C_D	-0.3	-	Parameter reflecting decreasing voltage when battery is progressively discharged
D_D	165	-	Parameter reflecting sharp decrease of voltage when battery is discharged to a low SOC
EF_D	1.25	-	Exponential factor introduced to achieve a closer curve fit for voltage behaviour when progressively discharged
C_1	0.0006	h/A^2	Parameter to calculate maximum charge capacity
C_2	0.0543	h/A	Parameter to calculate maximum charge capacity
C_3	2.0279	h	Parameter to calculate maximum charge capacity
C_4	140.29	Ah	Parameter to calculate maximum charge capacity
D_1	-0.0006	h/A^2	Parameter to calculate maximum discharge capacity
D_2	0.0543	h/A	Parameter to calculate maximum discharge capacity
D_3	-2.0279	h	Parameter to calculate maximum discharge capacity
D_4	140.29	Ah	Parameter to calculate maximum discharge capacity
B_s	36	-	Number of series batteries

Acknowledgements

I would like to express my sincere gratitude to may tutor, Profs Berkouk Elmadjid and Dr. Ghedamsi Kaci without whom none of this would ever have happened. Their professional supervision, insightful mentoring, encouragement and vast help steered the undertaken research into right direction.

References

[1] L. Hassaine, E. Olı´as, Simulation of grid-interface connecting photovoltaic power systems. Proceedings of the World Renewable Energy Congress IX Florence, Italy, 2006

[2] N. Hamrouni_, M. Jraidi, A. Che´ rif. New control strategy for 2-stage grid-connected photovoltaic power system. Renewable Energy 33 (2008) 2212–2221

[3] A. AL-Amoudi, L. Zhanc, Optimal control of a grid-connected PV system for maximum power point tracking and unity power factor. On power electronics and variable speed drives. Seventh International Conference on (Conf. Publ. No. 456), London, 1998, pp. 80–85

[4] Wu T-F, Nien H-S, Shen C-L, Chen T-M. A single-phase inverter system for PV power injection and active power filtering with nonlinear inductor consideration. Transactions on Industry Application 2005 Jul–Aug;41(4):1075–83

[5] Dali M, Belhadj J, Roboam X. Hybrid solar-wind system with battery storage operating in grid connected and standalone mode: control and energy management-experimental investigation. Energy 2010;35(6):2587-95

[6] Pouresmaeil E, Montesinos-Miracle D, Gomis-Bellmunt O, Bergas-Jané J.A multi-objective control strategy for grid connection of DG (distributed generation) resources. Energy 2010;35(12):5022-30

[7] Anna Rita Di Fazio, Mario Russo. Photovoltaic generator modelling to improve numerical robustness of EMT simulation. Electric Power Systems Research 83 (2012) 136– 143

[8] Hohm DPM, Roop ME. Comparative study of maximum power point tracking algorithms. Progress in Photovoltaic: Research and Applications 2003;11: 47-62

[9] Benjamin Wichert. Control of Photovoltaic Diesel Hybrid Energy Systems. PHD thesis of the Curtin University of Technology. 2000

[10] S. Armstrong, M. E. Glavin, and W. G. Hurley, .Comparison of battery charging algorithms for stand-alone photovoltaic systems. IEEE Power Elect. Specialists Conference, 2008, pp. 1469-1475.

[11] Alberto Lega. Multilevel Converters: Dual Two-Level Inverter Scheme. Ph.D. thesis. University of Bologna March 2007.

[12] J.S. Lai, F.Z. Peng, Multilevel converters : a new breed of power converters. IEEE Transactions on Industry Applications 32 (May (3)) (1996),pp. 509–517.

[13] N. Celanovic. Space vector modulation and control of multilevel converters. PhD thesis, Virginia Polytechnic Institute and State University, Blacksburg, Virginia, USA, 2000.

[14] Lalili D. Berkouk E. M., Boudjema F. , Lourci N.,Taleb T. and Petzold, J. Simplified space vector PWM algorithm for three-level inverter with neutral point potential control, The Medeteranean Journal of Measurement and Control. vol 3, No 1, (2007), pp.30-39.

[15] F. Blaabjerg, R. Teodorescu, M. Liserre, and A. Timbus. Overview of Control and Grid Synchronization for Distributed Power Generation Systems. IEEE Trans. Ind. Electron., vol. 53, no. 5, pp. 1398-1409, Oct. 2006.

[16] Bouchafaa F, Beriber D, Boucherit M.S. Modeling and control of a gird connected PV generation system. In: 18th Mediterranean Conference on Control & Automation, 2010. pp. 315–320.